Master's Thesis
석사 학위논문

High Efficiency Crumpled CNT Thin Film Heater For Hydrogen Sensing

Jeonhyeong Park (박 전 형 朴 全 泂)

Department of
Robotics Engineering

DGIST

2020

Master's Thesis
석사 학위논문

High Efficiency Crumpled CNT Thin Film Heater For Hydrogen Sensing

Jeonhyeong Park (박 전 형 朴 全 泂)

Department of
Robotics Engineering

DGIST

2020

High Efficiency Crumpled CNT Thin Film Heater For Hydrogen Sensing

Advisor: Professor Hoe Joon Kim
Co-advisor: Professor Hyuk-Jun Kwon

by

Jeonhyeong Park
Department of Robotics Engineering
DGIST

A thesis submitted to the faculty of DGIST in partial fulfillment of the requirements for the degree of Master of Science in the Department of Robotics Engineering. The study was conducted in accordance with Code of Research Ethics[1]

12. 20. 2019

Approved by

Professor Hoe Joon Kim (signature)
(Advisor)

Professor Hyuk-Jun Kwon (signature)
(Co-Advisor)

[1] Declaration of Ethical Conduct in Research**:** I, as a graduate student of DGIST, hereby declare that I have not committed any acts that may damage the credibility of my research. These include, but are not limited to: falsification, thesis written by someone else, distortion of research findings or plagiarism. I affirm that my thesis contains honest conclusions based on my own careful research under the guidance of my thesis advisor.

High Efficiency Crumpled CNT Thin Film Heater For Hydrogen Sensing

Jeonhyeong Park

Accepted in partial fulfillment of the requirements for the degree of Master of Science.

11. 26. 2019

Head of Committee Prof. Hoe Joon Kim (signature)

Committee Member Prof. Hyuk-Jun Kwon (signature)

Committee Member Prof. Sanghoon Lee (signature)

MS/RT
201823010

박 전 형. Jeonhyeong Park. High Efficiency Crumpled CNT Thin Film Heater For Hydrogen Sensing. Department of Robotics Engineering. 2020. 51p. Advisors Prof. Hoe Joon Kim, Co-Advisors Prof. Hyuk-Jun Kwon

ABSTRACT

This paper presents the fabrication of crumpled carbon nanotube (C-CNT) thin film heaters and its application towards high sensitivity and low drift hydrogen gas sensing. By utilizing a simple spray coating of pristine multi-walled carbon nanotubes (MWCNTs) and thermal substrate shrinkage method, we have fabricated a C-CNT film with closely packed junctions. Joule heating of C-CNTs results higher temperature at a given input voltage compared to as-deposited CNTs. Specifically, the temperature of C-CNT heaters increase as high as 200 % than as-deposited CNT heaters due to higher junction densities in a given area. In addition, the temperature coefficient of resistance (TCR) of both C-CNT and as-deposited CNT heaters are analyzed for an accurate temperature control and measurement of the CNT heaters. All of the fabricated heaters exhibit linear TCR, and thus allowing a stable thermal operation.

The higher heating efficiency of the C-CNT heaters can contribute to gas sensing with improved adsorption and desorption characteristics. Our results show that the C-CNT heaters are capable of hydrogen gas sensing while demonstrating higher measurement sensitivities along with lower drift compared to as-deposited CNT devices. Additionally, the self-heating mechanism of proposed heaters help rapid desorption of hydrogen, and thus

allowing repetitive and stable sensor operation. Our findings reveal that both CNT morphologies and heating temperature affect the hydrogen sensing performances. The proposed C-CNT devices are suited for low power or voltage sensing platforms.

For future work, sub-mm scaled shadow masks would allow C-CNT devices to be scaled down to μm-scale from macro-scaled devices. Hence, we envision the batch fabrication of C-CNT device arrays. In addition, C-CNT structures will be onto thermally resistant substrates, such as Silicon wafer, Glass or PET, so that we can compare C-CNT devices with as-deposited CNT on same substrate. Utilizing SEM micrographs and Raman analysis, the proposed transfer printing process will be optimized as well.

List of Contents

List of Table

List of Figures

1. INTRODUCTION

Since the discovery of carbon nanotubes (CNTs) by Iijima in 1991, CNTs have drawn large attention with outstanding properties [1-3], such as high electrical and thermal conductivity, high mechanical strength, and interesting optical features. For example, CNTs can carry three times more current than copper. Furthermore, research demonstrates that CNTs have high thermal conductivity of approximately 3500 W/m·K at room temperature. In terms of mechanical properties, an elastic modulus of about 1 TPa and a tensile strength of about 100 GPa has been measured for individual CNT [1].

CNTs, the walls of which consist of hexagonal lattice of carbon atoms, are cylinder shaped macromolecules. Interestingly, CNTs are made up with high aspect ratio, in which their range of diameters could be 0.5 nm to more than 20 nm with lengths of several centimeters, as shown in figure 1(a). CNTs are divided into Single-walled CNTs (SWCNTs) and Multi-walled CNTs (MWCNTs). SWCNTs generally have a diameter range of 0.5 nm to 12 nm with different tube lengths, which starts with a few micrometers depending on the manufacturing process and treatment techniques. On the other hand, MWCNTs consist of multiple rolled layers of hexagonal lattice of carbon atoms (graphene), and they can reach more than 25 walls with a spacing of 0.34 nm. The outside diameters of MWCNTs ranges from 1 nm to 50 nm [2]. The growth of MWCNTs is much easier than that of SWCNTs, and thus MWCNTs are better suited for mass production. In addition, individual CNTs can contain not only metallic but also semiconducting properties depending on the orientation of nanotube axis with respect to the hexagonal lattice, which is chirality. Specifically, the geometric arrangement of carbon atoms is classified into armchair (n=m) or zigzag (m=0). Whereas aforementioned both types of CNTs have mirror symmetry, asymmetric structures are nanotubes with $m \neq n$, as shown in figure 1(b-c).

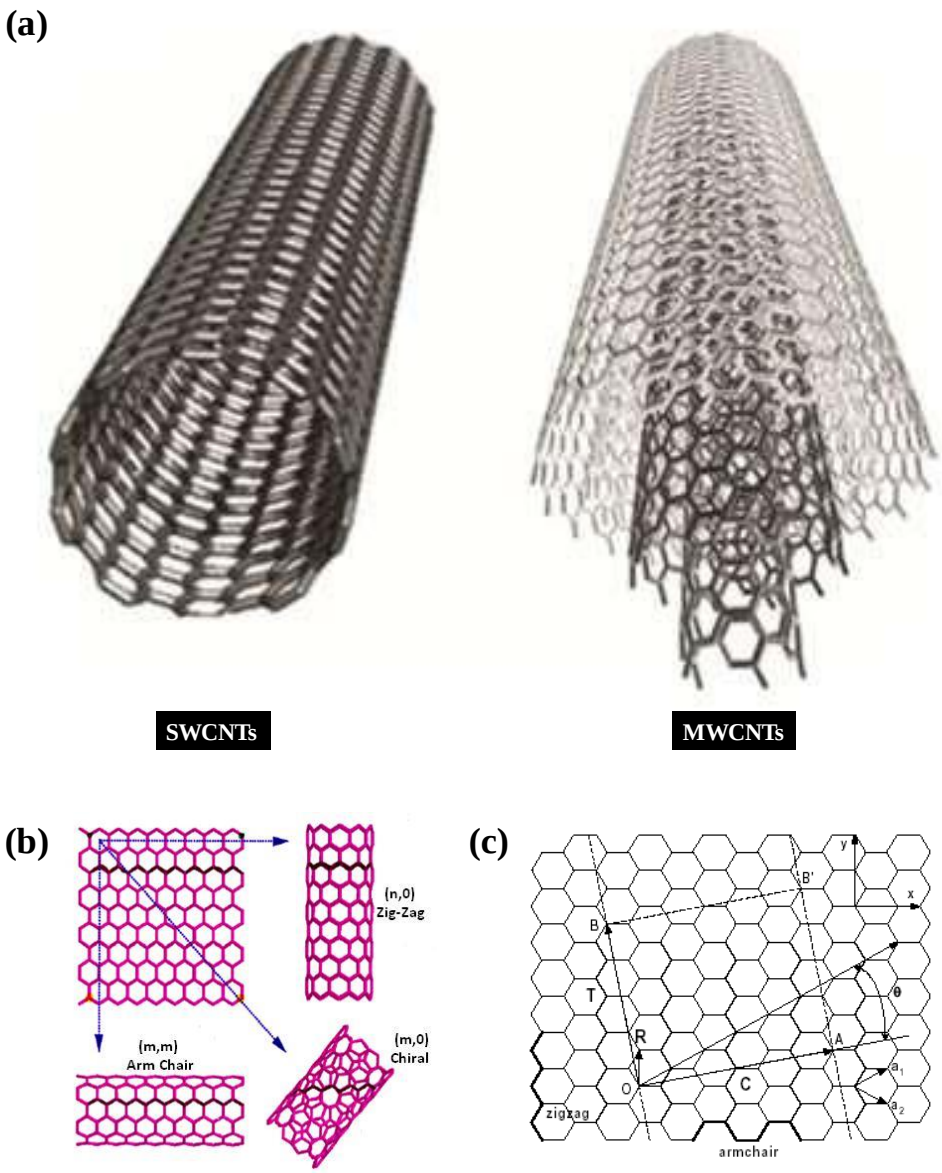

Figure 1. (a) Schemaic of SWCNTs and MWCNTs [4] (b) CNT charlity depending on oreientation of nanotube axis (Three different classifications are shown), and (c) The chiral vector of CNTs [2]

1.1. CNT Based Sensors & Electronic Device

Utilization of outstanding electrical properties of CNTs would allow the development of next generation electronics or embedded systems [2]. In building transistors, one can use both semiconducting and metallic properties of CNTs. For example, semiconducting CNTs can consist the main transistor, while metallic nanotubes form conducting electrodes. However, the accurately controlling the proportion semiconducting or metallic CNTs are

challenging and ultimately limiting the commercialization of CNT integrated devices. Therefore, a scalable method to control the electrical properties of CNTs should be developed.

The gas sensing mechanism strongly relies on the adsorption and desorption of gas molecules on sensing materials with charge transfer between them. CNTs can be one of the desirable nanomaterials for gas sensing. This is because large surface area of CNTs allows more gas molecules to be absorbed, which is favorable for charge transfer. However, due to large binding energy between CNT and gas molecules, rapid recovery can be a critical issue for CNT based gas sensors. To overcome such a limitation, an external energy (i.e. UV light illumination, high vacuum condition, and thermal energy) often applied to enhance the recovery time of the sensors [5, 6].

In addition to the aforementioned applications of CNTs, there has been growing attention in using them as heating elements [3]. A number of materials, such as tin oxide (ITO), Ni-Cr (Nichrome), or Fe-Cr-Al (Kanthal) have been employed for heating devices, but they have numbers of limitations, such as a heavy weight, rigidity, brittleness, and intolerance to acids and bases. CNTs possess excellent electro-thermal properties, not to mention the fact that they are tolerant against harsh environment as well as mechanical forces.

1.2. Specific Aims of Thesis

This thesis consists of two main goals: (1) enhancing the heating efficiency of CNT thin film heaters, and (2) hydrogen gas detection by developing crumpled CNT heaters. First, we have fabricated crumpled CNT thin film heaters by thermal substrate shrinkage and characterized them in comparison with as-coated CNT thin film heaters on un-shrunk flexible substrates. We have verified that thermal substrate shrinkage increases junction density in a given area, leading to less heat loss while joule heated. Furthermore, we have analyzed temperature coefficient of resistance (TCR) and the power efficiency of as-deposited and

crumpled CNT heaters. The efficient heating capabilities of fabricated C-CNT heaters are favorable for hydrogen sensing with good desorption characteristics. By accomplishing these two main goals, we are able to develop CNT based heaters and electrochemical sensors towards ultra-low power and high sensitivity hydrogen gas sensing.

2. Background/Review of Relevant Previous Work

2.1. Operating Principles & Outstanding Advantages of CNT Heaters

Figure 2(a) shows Scanning Electron Microscope (SEM) images of MWCNTs pulling from MWCNT forest. This forest can be fabricated by chemical vapor deposition (CVD) [4] with well-controlled gaseous environments using Acetylene (C_2H_2), Hydrogen (H_2), and Helium (He) [7]. CNTs are randomly entangled when dispersed into a solvent. Such unique morphology of CNTs can result in high junction resistance, causing a large increase in temperature when joule heated. As CNTs can be deposited and patterned on a flexible polymer substrate, CNT based thin film heaters have drawn much attention. Figure 2(b) shows the schematic of a fabricated MWCNT thin film heater. Their electro-thermal properties strongly rely on the amount of deposited CNT. Specifically, the amount of CNTs determines the number of junctions, which results in joule heating upon applying a current. Furthermore, the optical transparency can be controlled by adjusting CNT thicknesses, and thus enabling the fabrication of highly transparent CNT thin film heaters. In addition, CNTs heaters show good temperature uniformity on the substrates because of uniform deposition methods of CNTs. [8]. Thus, we envision that CNT heaters could be utilized as the future film heater. [3, 7]. For example, potential application areas include the defrosters in windows, battery warmer for electric vehicles, and wearable systems.

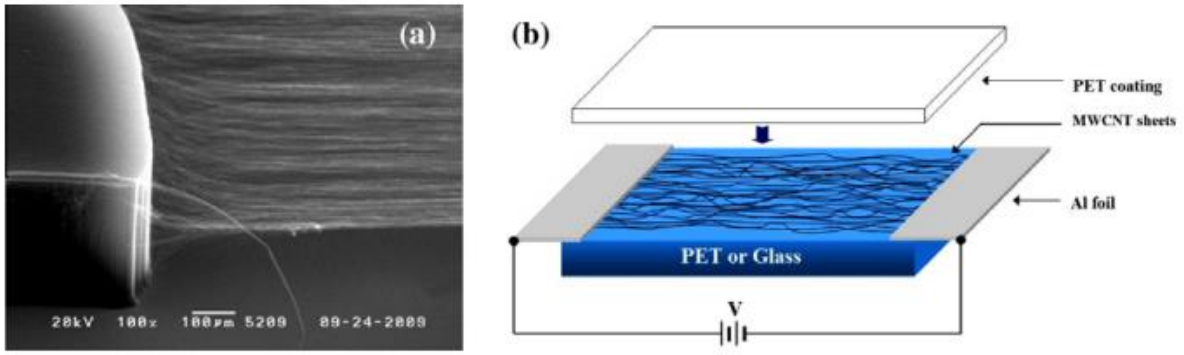

Figure 2. (a) SEM images of MWCNTs pulling from MWCNT forest (b) The diagram of MWCNT sheets on a substrate with electrodes [7]. CNT thin film heaters require high operation voltage to be heated due to high electrical resistance

2.2. Improving the Performance of CNT Thin Film Heaters

2.2.1. Chemical Treatment and Nanoparticle Deposition

Previous researches show that the performance of CNT thin film heaters can be improved by a chemical treatment or a deposition of metal nanoparticles [9]. CNTs possess numbers of disjoint individual CNTs due to defects and amorphous carbon, as shown in figure 3(a). To eliminate them, the mild acid treatment has been used, resulting in highly interconnected individual CNTs (figure 3(b)). As a result, this method has improved heating performances of CNT based heaters.

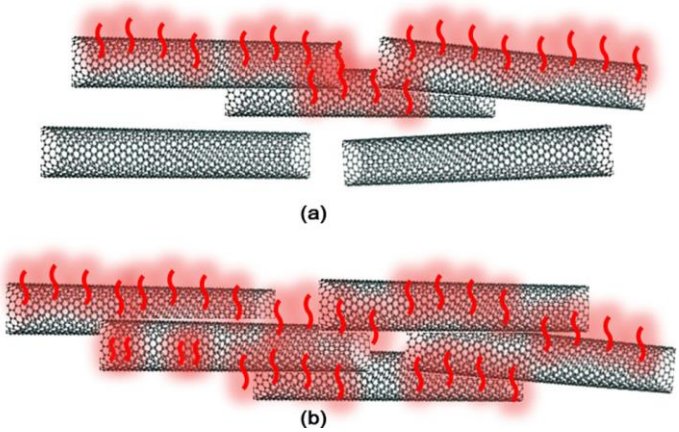

Figure 3. Schamatic views of disjointed and jointed CNTs (a) before and (b) after the mid acid treatment respectively [9].

In addition, the metal nanoparticles, especially Nickel (Ni), have been deposited on CNT layer because Ni nanoparticles can be easily synthesized under the room temperature, as shown in figure 4(a-c). By using electro-deposition method, metal nanoparticles can lead to hundreds or thousands connections of CNT junctions, which can induce an increase in electrical resistance due to discontinuities of Ni nanoparticles. Thus, the effective thermal energy can be generated from both CNT junctions and metal nanoparticles, as shown in figure 4(b).

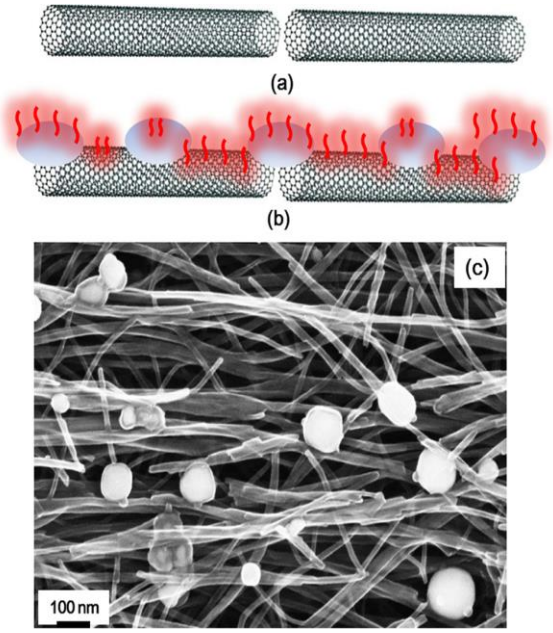

Figure 4. Schematic and SEM images of (a) before and (b-c) after metal nanoparticle deposition [9]

2.2.2. Doctor-blade Method Deposition and Increase in Power Efficiency

For a large area transparent CNT thin film heater, doctor-blade fabrication process has been proposed as a new deposition method [10]. This deposition method enables CNT layer to be deposited on a large area with a desired thickness by controlling the precise gap between the blade and substrate. Additionally, this fabrication process is applicable to a wide range of substrates, and even flexible polymer substrates, as shown in figure 5.

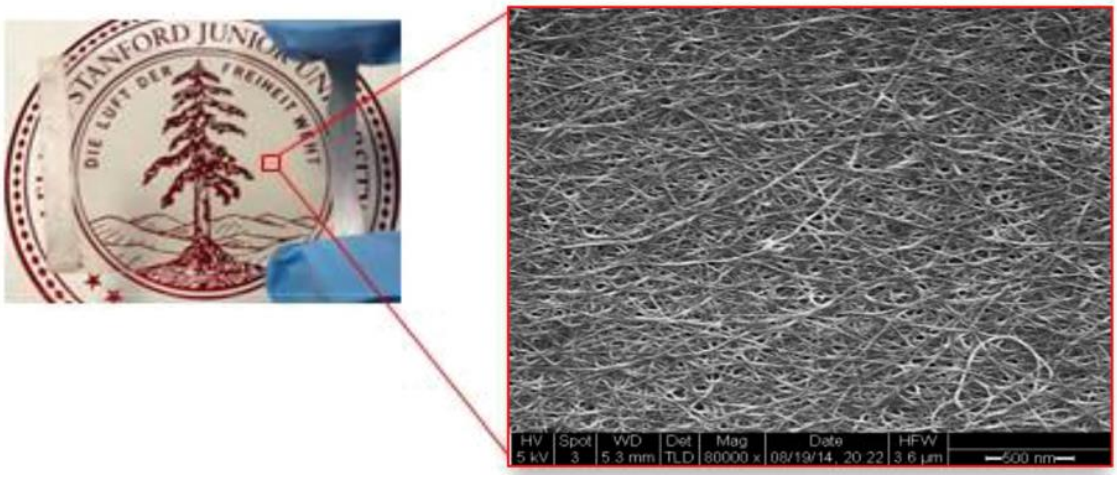

Figure 5. Photograph and SEM images of transparent SWCNT heaters on a plastic substrate [10]

Furthermore, Kim et al [10] point out that the heat capacity of substrate can affect the response speed and saturation temperature of heaters, then they have utilized an extremely thin polymer substrate (12 μm PEN, 1100 J/kg·K) which is lower thermal capacity than other conducting sheet. The power consumption (dT/dP) of the CNT heaters exhibits 187 ℃/W·cm^2, which is much larger than other published results [11-13].

2.3. Densified Structure by Substrate Shrinkage Method

For improving the heating efficiency of CNT based heaters by less heat loss and more connections of CNT junctions, the fabrication of densified CNT structure is needed. Previous studies [14-16] have shown the utilization of shrinkable shape memory substrate to control the densification. Specifically, polystyrene (PS) film starts shrinking bi-axially when absorbing the heat above glass transition temperature, which is about 150 ℃ without any restriction [14]. For example, when metal nanowires are deposited on PS film and clamped on two sides as shown in figure 6(a-b), the substrate shrinks in one direction, which can result in highly densified structure of nanowires.

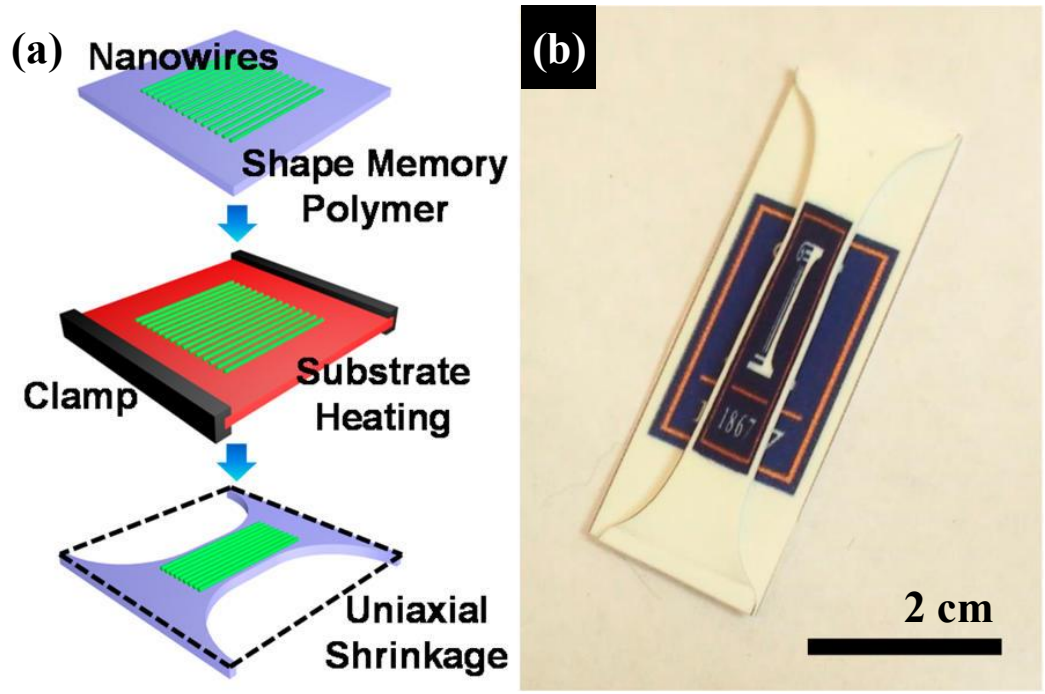

Figure 6. (a) Schemiatic view of shrink-induced nanowire assembly process. (b) Photograph of PS film after uniaxial shrinkage

The integration of CNTs and shrinkable polymer substrates has been also studied for thin film strain sensors [15]. The fabrication of CNT strain sensors starts with a spray deposition of CNTs on PS thin film with a shadow mask. The area of as-deposited CNT thin film reduces upon heating using a convection oven, which results in densified CNT structure. To fabricate stretchable CNT sensors, densified CNT structure has been spun on a soft silicone elastomer, such as Ecoflex 0030 or PDMS, followed by etching PS film by acetone and toluene. After completing the fabrication, this work demonstrates reproducibility of suggested CNT strain sensors with strain ranging 100 % to 300 %, which corresponds to hysteresis response of 1 % to 7 %. As shown in figure 7, tightly entangled CNT sensors can sustain up to 400 % without discontinuities of CNTs [15]. According to the suggested CNT models, authors have point out that the highest localized stress would be above 400 % where the fractures of densified CNTs occur.

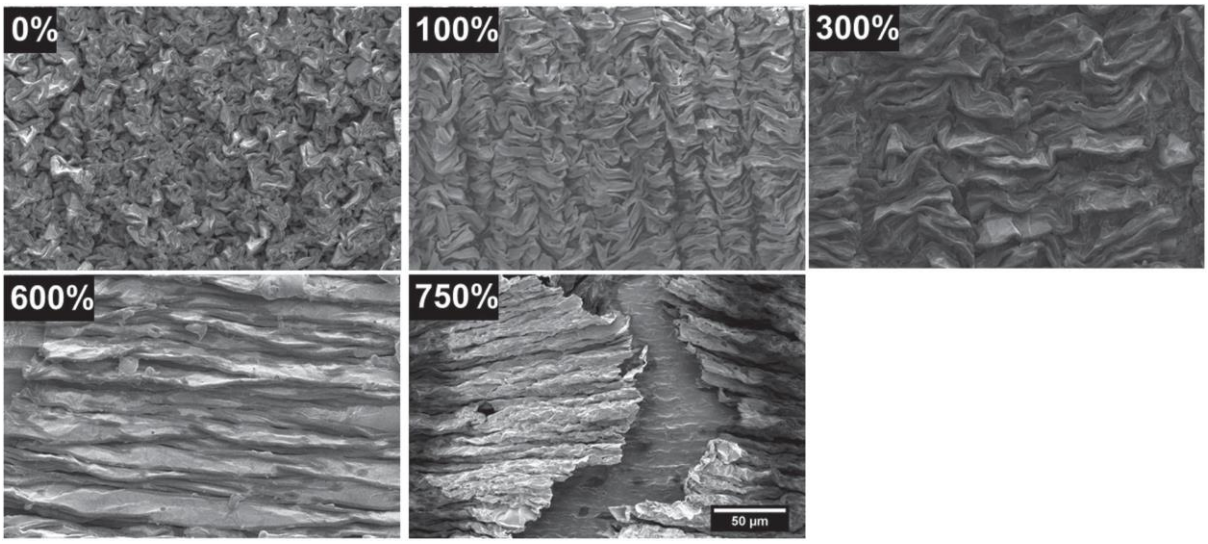

Figure 7. SEM images of densified CNT thin film sensors on a silicone elastomer substrate with different strains [15]

Another method to fabricate crumpled structure of CNTs is to utilize stretchable elastomer substrate [17], as shown in figure 8(a). After the growth of vertically aligned CNTs by plasma enhanced CVD (PECVD) as shown in figure 8(b), as-grown CNT forest should be annealed at temperature of 490 ℃. This is because most CNTs can be broken at the interface of tubes against the catalysts (Fe), which can result in easy detachment of CNT forests from silicon wafer. This pretreated CNT forest is stamped on the pre-stretched substrate with clamping edges. The pre-applied strains can be either uniaxial or biaxial to fabricate uni-axially or bi-axially stretchable electronic devices. The wafer is then peeled off from the pre-strained substrate. Subsequently, this substrate returns to original shape with holding the stamped CNT forest along with one or two directions. Figure 8(c) shows uni-axially deformed CNT forest on an elastomer substrate after relaxation. Self-assembled CNT forest with biaxial relaxation can be also fabricated due to mismatching the different material properties of CNT forest and elastomer substrate, shown in figure 8(d).

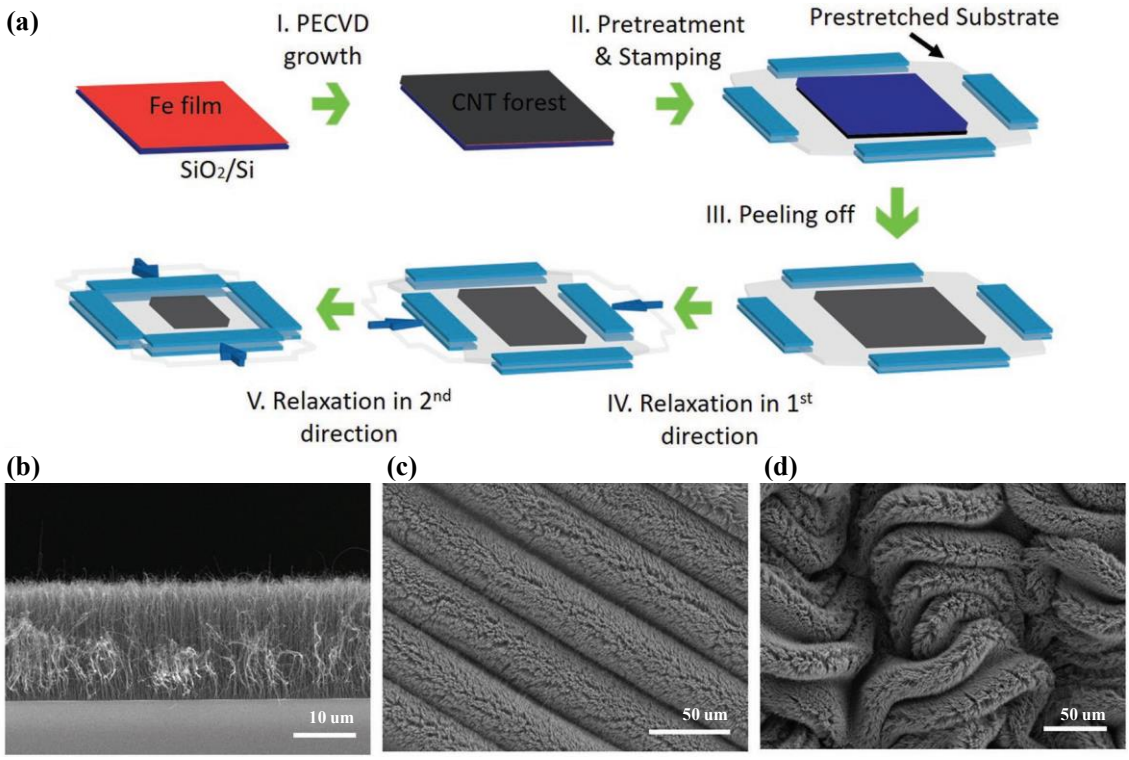

Figure 8. (a) The whole fabrication process of crumpled CNT forest, (b) SEM image of the growth of CNT forest by PECVD, (c) SEM image of uniaially relaxed CNT forest, and (d) SEM image of biaxially relaxed CNT forest [17].

2.4. CNT based Gas Sensors

For developing electrochemical sensors, CNT based gas sensors have significantly drawn attention owing to their high sensitivity, simple fabrication process, and fast response time [18, 19]. Out of several existing detection mechanisms, the chemiresistive-sensing scheme is most widely used, as it is power efficient and easy to adapt with existing electronic components [20, 21]. MWCNTs based chemiresistive sensors exhibit semiconducting properties along with high surface to volume ratio, and thus enabling the high measurement sensitivities [22, 23]. Previous research have covered from the development of single CNT wire integrated transistor type sensors [24, 25] to flexible sensors for wearable applications [26]. Furthermore, the scalable production of CNT based gas sensors have been allowed from a number of economical methods, such as direct-growth, transfer printing, and spray coating

and spin coating process [27-29]. Even though CNT based gas sensors possess numerous aforementioned benefits, these sensors still need to overcome in terms of measurement reliability or ability to make repetitive measurement [30, 31].

In chemiresistive sensing mechanism, the adsorption or adhesion of gas molecules onto CNT leads to shift in its electrical resistance [6, 19]. The adsorbed gas molecules should be removed from CNT surfaces when the gas does not flow over CNT, so that it can make reliable and repetitive measurement. At room temperature, the perfect desorption requires long time, and even causes permanent shift in the electrical resistance of sensors [5, 32]. Such drift issue in electrical resistance is undesired, particularly in applications where one needs to make repetitive and lengthy measurements. However, the desorption process can be expedited through utilizing external energy sources [33], such as high vacuum operation, UV light induced photo desorption, or thermal annealing. Generally, thermal energy has been widely used to mitigate the drift of CNT based gas sensors due to its simplicity. For instance, once the temperature of 100 ℃ applies to CNT hydrogen gas sensors, the electrical resistance of the sensors rapidly recovers towards original value [34].

As mentioned previously, since CNT layers can work as a joule heater, such platform can be ideal for gas sensing applications at elevated temperatures. Furthermore, the heating properties of CNT heaters rely on the amount of CNT junctions at a given area or volume due to joule heating mechanism at CNT junctions [7, 35, 36]. Thus, higher junction densities lead to more power heating efficient, and the compressive or crumpled CNT structure can significantly increase the junction densities.

Here, we suggest the fabrication of crumpled CNT (C-CNT) heaters using a simple spray coating and thermal substrate shrinkage method, which is followed by the characterization of electrical and thermal properties of the heaters. Then, we detect hydrogen gas by using C-CNT heater, and analyze the measurement sensitivity, drift in sensor

resistance, repeatability, and temperature dependent sensor operation. Finally, we compare the performance of C-CNT sensors to as-coated CNT platform to point out the advantages of the proposed C-CNT platform.

3. Materials and Methods

3.1. Fabrication of Crumpled CNT Device

CNT thin film heaters rely on localized heat generation at a number of CNT junctions when current flow through CNT mesh networks [3]. High junction resistances induce rapid increase in temperature. The proposed CNT device utilizes such joule heating mechanism and consists of CNT layer on top of 200-μm-thick polymer substrate, and 100-nm-thick-metal electrodes, as shown in figure 9(a). To make direct comparison between conventional as-coated CNT heaters and C-CNT heaters, we have utilized two different substrates of Polyethylene Terephthalate (PET) and Polystyrene (PS) films. PET is thermally resistant while PS shrinks about 50 % in length when heated up to above 120 ℃ [14]. The initial amount and deposition area of CNTs are equivalent for both PET and PS substrates. However, the final sizes are different due to thermal substrate shrinkage.

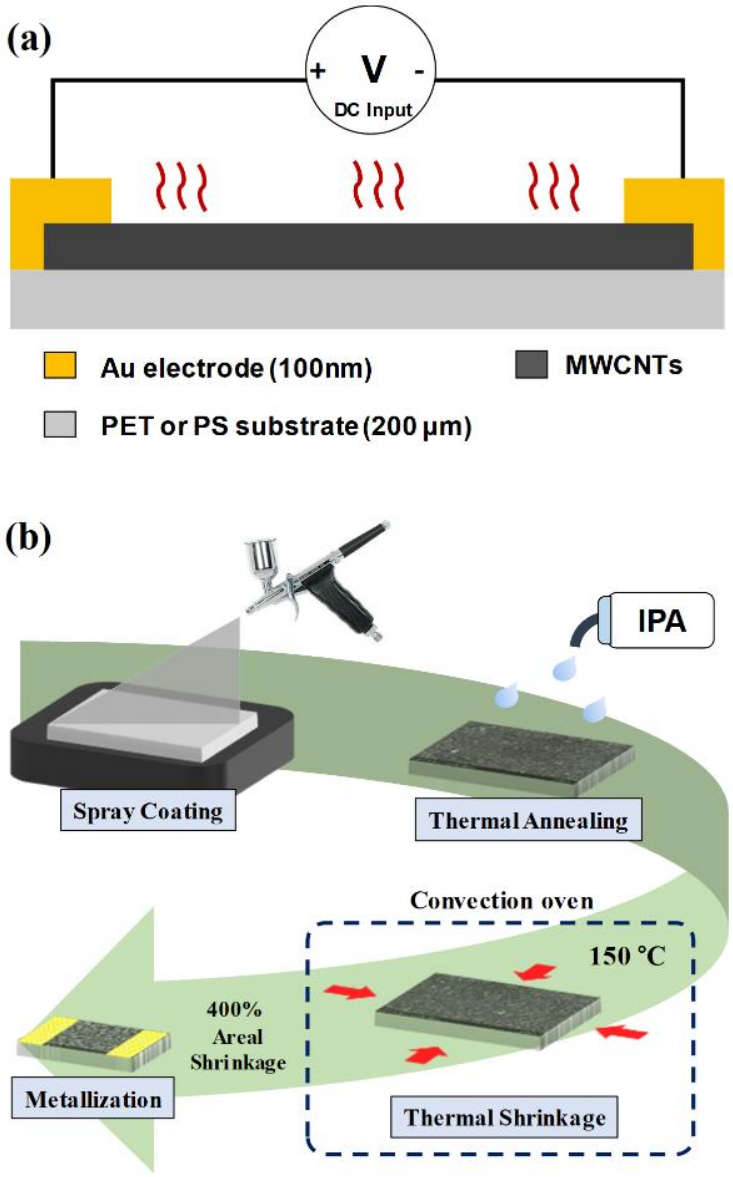

Figure 9. (a) A schematic of the crumpled and as-coated CNT heaters. (b) Fabrication process including CNT spray deposition, thermal annealing, shrinkage method of PS substrate, and metallization for electrodes.

Figure 9(b) illustrates the overall fabrication process of C-CNT heaters. Initially, a 3 wt% MWCNT solution is diluted in isopropyl alcohol (IPA), and then spray coated for 10 seconds at the flow rate of about 0.4 mL/sec. The heater is then rinsed with IPA for removing any defects on deposited CNT. After the cleaning process, the heater is placed inside the convection oven at 70 ℃ for 30 minutes to remove any IPA vapors that can remain in CNTs.

This thermal annealing process enhances the adhesion between CNTs and the polymer substrates. For fabricating crumpled CNT structure, the device fabricated on PS substrate is heated at the temperature of about 150 ℃ for 5 minutes using air convection oven. The heater size reduces by about 400 % in area after thermal substrate shrinkage. Lastly, a layer of silver paste followed by a 100-nm-thick metal layer (Au or Pt) is sputter deposited at the sides of device to form electrodes.

Table 1 provides the shrinkage properties and parameters of aforementioned polymer substrates. As mentioned previously, PET does not shrink despite applying the heat, because it is thermally resistant. However, once PS substrate reaches the glass transition temperature of above 120 ℃, it starts shrinking due to shape memory property.

Table 1. Thickness and Shrinkage Rate in area of each substrate

	PET	PS
Initial Thickness	188 μm	254 μm
Deformation Temperature	150 ℃	120 ℃
Shrinkage Rate in Area	NA	400%

3.2. Device Characterization and Hydrogen Sensing Setup

For an accurate temperature control and measurement, the electro-thermal properties of as-deposited CNT and C-CNT heaters are characterized. MWCNTs exhibit good linear temperature coefficient of resistance (TCR) [37], thus its temperature can be well calibrated from the measured electrical resistance. Specifically, TCR of all fabricated heaters are measured while monitoring the heater temperature using an infrared (IR) camera with applying various input voltages. To accurately measure the resistance of heaters ($R_{heaters}$), we have set up a simple circuit which consists of DC power supply, a 100 Ω sense resistor (R_{sense}), and CNT heaters. As shown in figure 10, such method enables the measurement of

$R_{heaters}$ by calibrating the voltage drop across R_{sense} (Equation (1)). The characterization of all CNT devices has been carried out at the room temperature of around 20 ℃ in a humidity-controlled environment.

$$R_{heater} = R_{sense} \times (V_{in} - V_{sense}) / V_{sense} \quad (1)$$

Figure 10 shows the experimental setup for hydrogen gas sensing. The experiment is performed inside the vacuum probe station with access to argon (Ar) and hydrogen (H_2) gases. We have set the gas flow rate of 500 sccm with 10 % hydrogen concentration, which corresponds to 450 sccm of Ar and 50 sccm of H_2 respectively. This hydrogen sensing has performed without sensor characterization as a function of varying hydrogen concentrations. The vacuum chamber has been maintained at 400 mTorr using the automatic purge valve control. Importantly, to minimize conduction heat loss, we have placed CNT sensors about 5 mm above the surface. Hydrogen gas is flowed into vacuum chamber after 7 minutes for both pressure and sensor temperature stabilization throughout the entire sensing experiments. Each sensing cycle is totally 8 minutes long. In other words, hydrogen gas is flowed 4 minutes towards the chamber and then turned off for another 4 minutes. By utilizing Labview program, we could record the heater resistance at every 100 ms as hydrogen adsorption would alter R_{heater} due to electron-hole recombination [38].

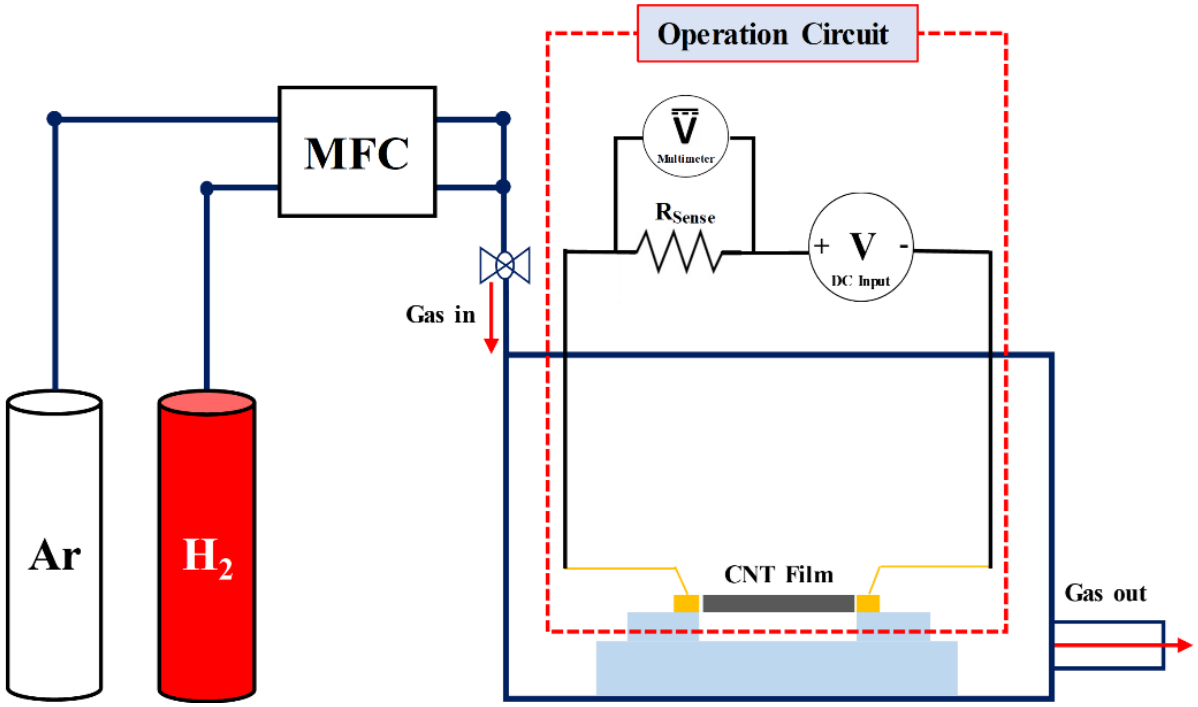

Figure 10. Experiment setup for hydrogen gas sensning and CNT heater operation. By measuring the voltage drop (V_{sense}) across the 100 Ω sense resistor (R_{sense}), the sensor resistance can be calibrated

4. Results

4.1. Device Characterization

Figure 11(a) shows the fabricated as-deposited CNT heater on a PET substrate and C-CNT heater on a shrunk PS substrate. The area of C-CNT device has reduced by about 400 % after thermal substrate shrinkage method. Although the initial area and amounts of deposited CNT are identical for both heaters, the C-CNT heater appears to be darker. This means that the areal density of CNTs have increased after the shrinkage. The resistance of CNT and C-CNT heaters are 12.4 kΩ and 5.1 kΩ respectively at room temperature. For heater working demonstration, we have attached a large scaled CNT heater on PET substrate to a beaker filled with water, as shown in figure 11(b). Figure 11(c) shows we also demonstrate good temperature uniformity of heater by using an IR camera. Both CNT and C-CNT heaters have shown stable thermal operation of up to 90 ℃ without any mechanical deformation or delamination of CNT layer.

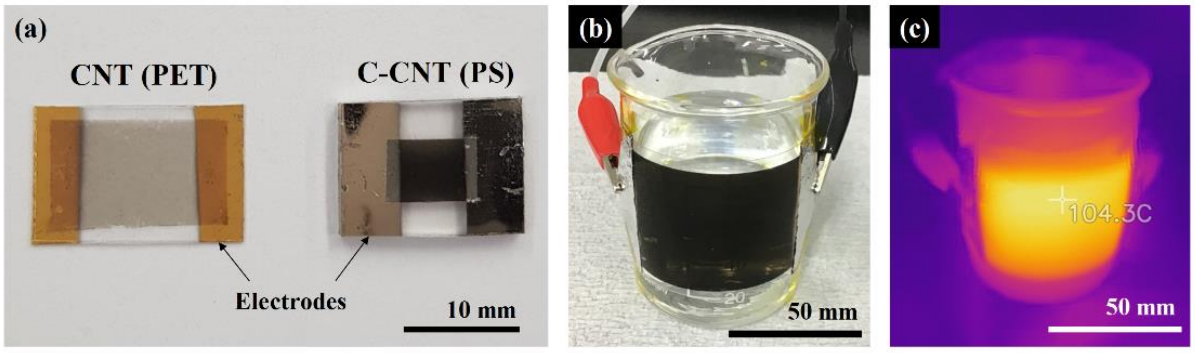

Figure 11. (a) Photographs of as-deposited CNT heater on a PET substrate and C-CNT heater on shrunk PS substrate. (b) Application of as-deposited CNT heater on a curved surface. (c) Infrared (IR) image of the CNT heater.

Figure 12(a-b) show scanning electron microscope (SEM) micrographs of as-deposited CNT and C-CNTs. C-CNTs shows higher densified bundles of CNT due to an area reduction

of PS substrate [15, 16], while air-spray deposited CNTs are randomly entangled. Additionally, there are more CNT junctions for C-CNT as compared to as-deposited CNT. This results in higher heating efficiency because of less heat loss between CNT junctions. As shown in figure 12(c), Raman analysis confirms that CNT quality does not degrade from thermal substrate shrinkage. This is because typical Raman peaks of CNTs (D-peak, G-peak, and 2D-peak) are present [39] with fairly consistent G-peak to D-peak ratio. In terms of as-deposited CNT heater, we can see PET Raman peak since Raman laser can go reach PET substrate. On the other hand, there is no PS peaks for C-CNT devices as the transparency considerably decreases with increased CNT densities per given area due to the thermal shrinkage process. This means that the proposed thermal shrinkage process is reliable and does not induce chemical transformation of the material.

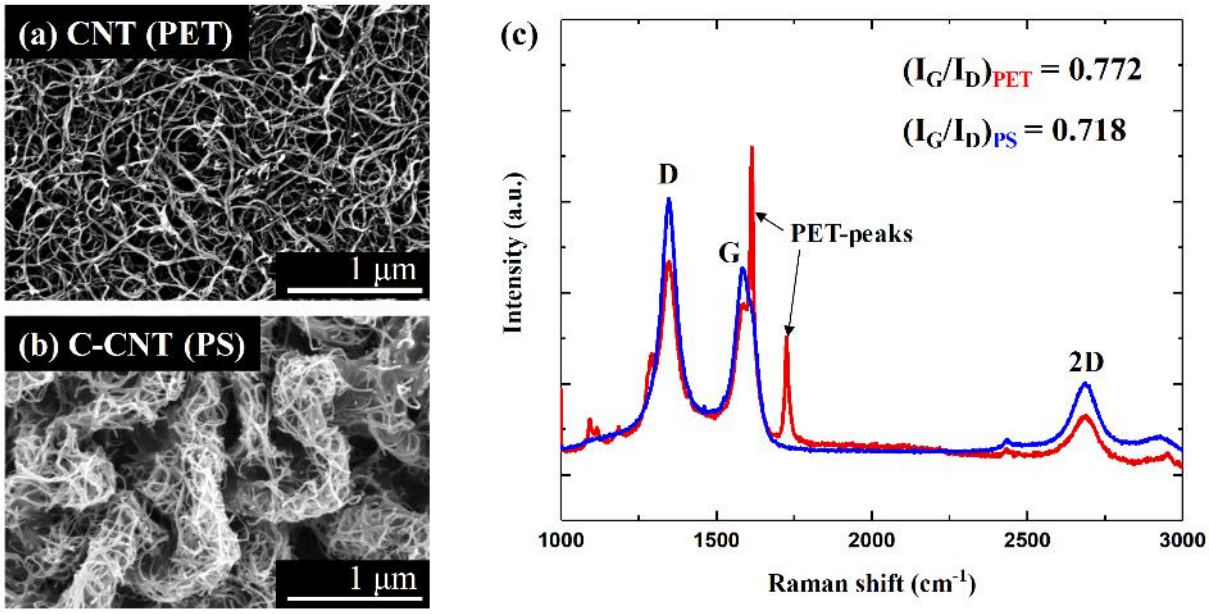

Figure 12. SEM images of (a) as-deposited CNT and (b) C-CNT. (c) Raman spectra of as-deposited CNT and C-CNT shows that thermal shrinkage does not affect the quality of CNT

Figure 13 shows the characterization of electro-thermal property for fabricated devices. Since C-CNTs exhibit higher junction densities, it demonstrates better heating efficiencies as

compared to as-deposited CNTs. C-CNT device shows higher increase in temperature than CNT device at a given voltage and power, as shown in figure 13(a-b). Such higher heating efficiency of C-CNT device is promising for enhancing not only the desorption of gas molecules but also the adsorption rate according to thermodynamics [31]. Figure 13(c) shows the change in electrical resistance as a function of temperature. For as-deposited CNTs, TCR is measured to be -892.0 ppm/℃. However, TCR of C-CNTs shows -590.5 ppm/℃. Obviously, MWCNTs possess both metallic and semiconducting tubes at the same times. A compressive stress caused by thermal shrinkage can change the chirality from semiconducting to metallic tubes [40], which can affect TCR of CNTs. Even though TCR shows shift after shrinkage method, both CNT and C-CNT devices exhibit good linear relation between heater resistance and temperature. This good linearity of TCR is quite favorable for an accurate temperature measurement and the control of fabricated device. Furthermore, a linear I-V relation means that the change in heater resistance is rather small while the devices are joule heated, as shown in figure 13(d).

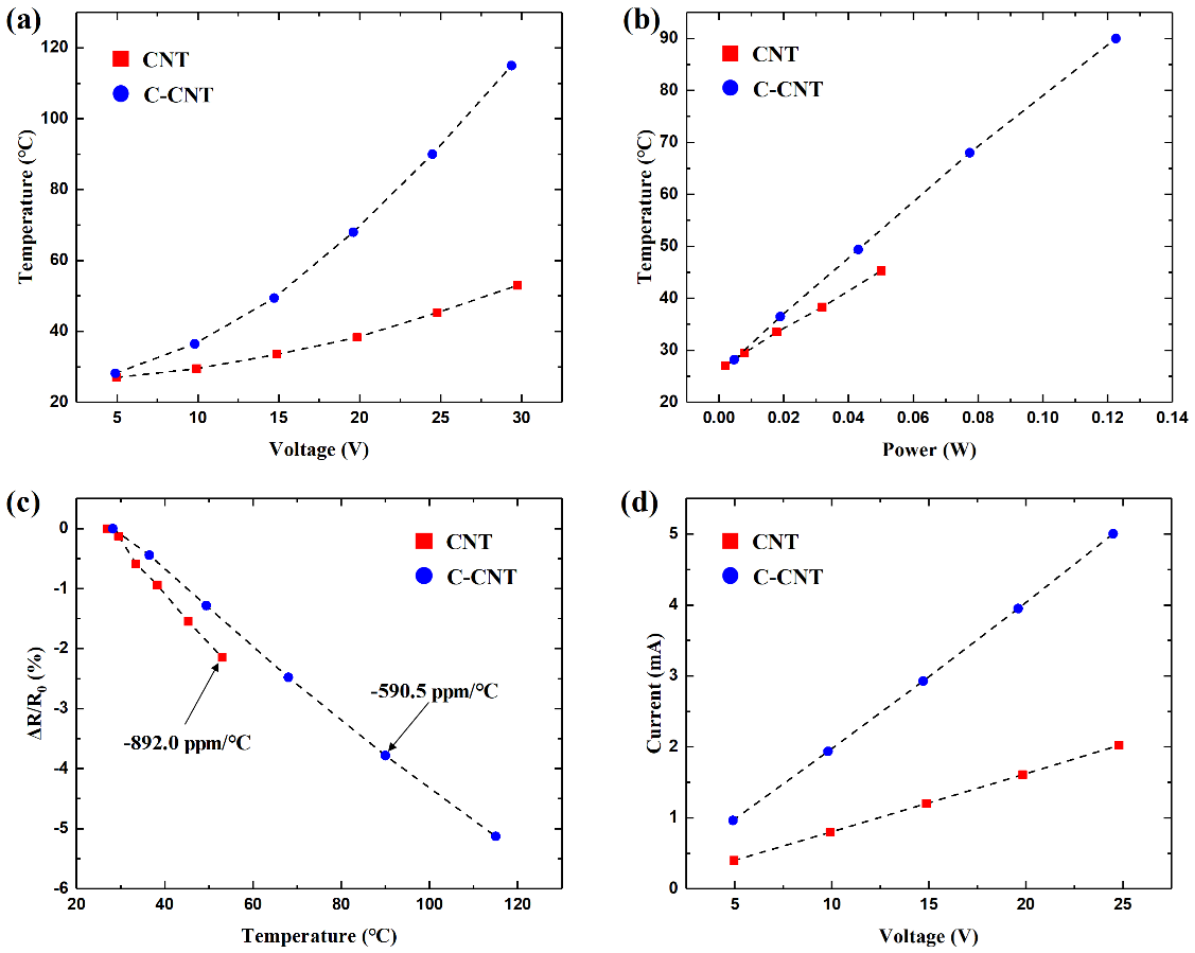

Figure 13. CNT device temperatures as a function of applied (a) DC voltage and (b) heater power. (c) Temperature coefficicient of resistance as a function of temperature. (d) I-V characteristics of the sensors

4.2. Hydrogen Gas Sensing

The fabricated CNT heaters can work as sensors to measure hydrogen gas. Figure 14 shows the response of both as-deposited and C-CNT sensors to 10 % concentration of hydrogen gas at room temperature of about 20 ℃. The sensitivity is defined as the equation (2), where R_0 is the initial resistance of CNT devices before detecting hydrogen. It is obvious that C-CNT sensor shows higher sensitivity along with more stable operation than as-deposited sensor. However, the range of measured sensitivity are about 0.01 %, and exhibits severe drift due to poor adsorption and desorption rates of hydrogen at ambient temperature.

$$\text{Sensitivity} = (R_{\text{heater}} - R_0) / R_0 \times 100\ [\%] \quad (2)$$

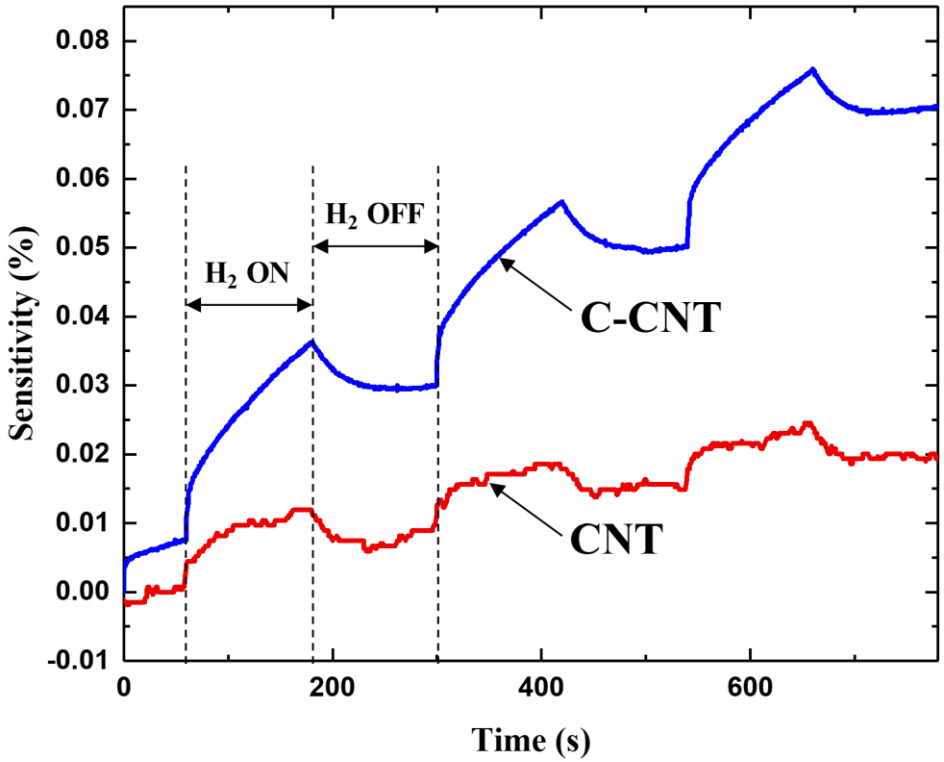

Figure 14. Hydrogen sensing response of CNT and C-CNT sensors without heating. Although C-CNT sensors shows higher sensitivity, a significant sensor resistance is shown.

In order to improve the rates of adsorption and desorption for hydrogen sensing, we have carried out the gas sensing experiment while both CNT and C-CNT sensors are self-heated. Figure 15(a-b) shows the change in sensitivities at input voltages of 10 V and 20 V. The heating temperature for C-CNT sensors are higher even at same input voltage due to the better heating efficiencies. The higher temperature while sensing can result in an increase in hydrogen adsorption rates, and consequently enabling high sensitive hydrogen response. For example, C-CNT sensors exhibit about 350 % improvement in sensitivity as compared to as-deposited CNT sensors at input voltage of 20 V, as shown in figure 15(c). Furthermore, the measurement sensitivities have considerably enhanced at elevated sensor temperature

compared to hydrogen gas detection in room temperature. This indicates that self-heating mechanism is not only relatively simple, but also quite effective for high sensitivity of hydrogen gas sensing.

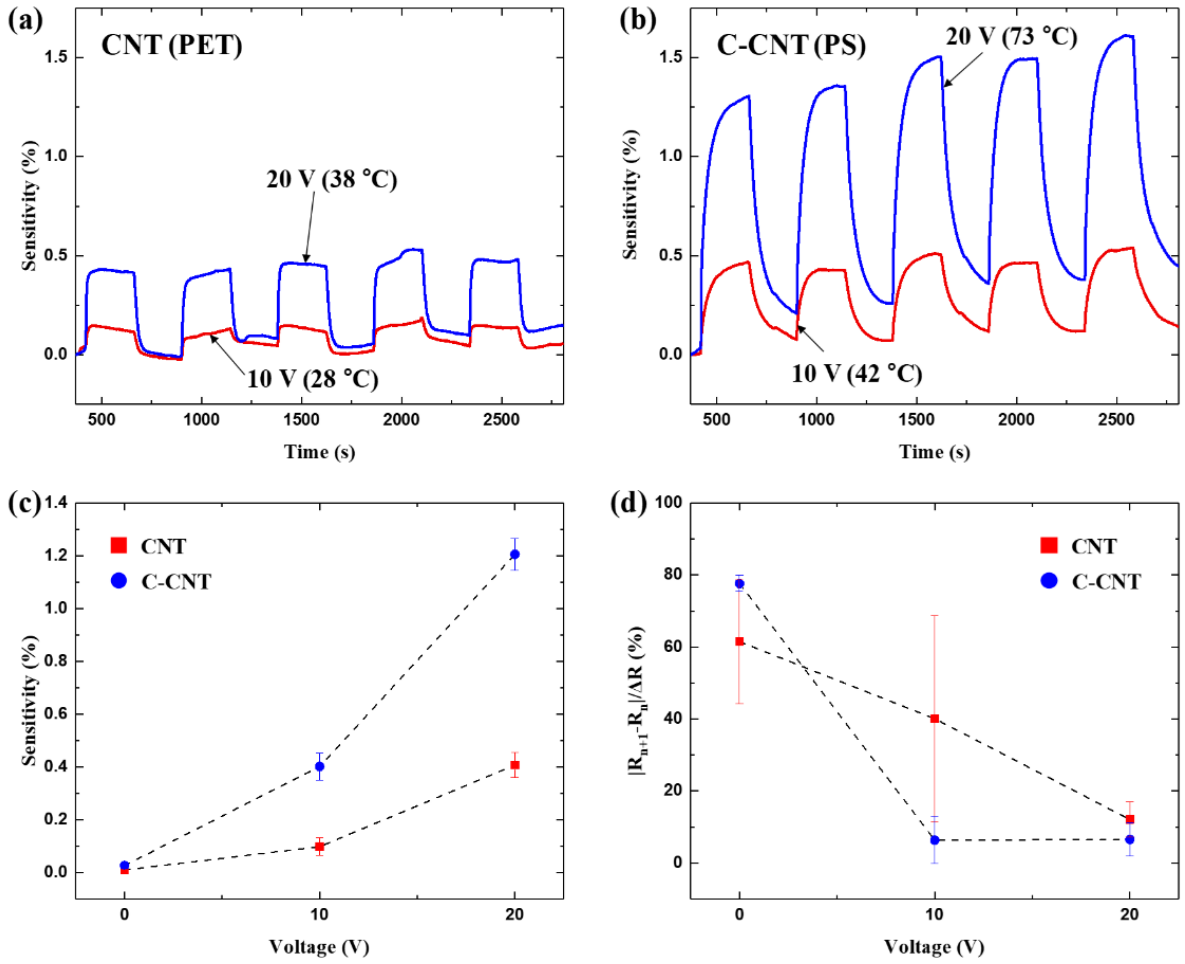

Figure 15. The response of hydrogen sensing with 10 and 20 V input voltages for (a) CNT and (b) C-CNT sensors. (c) Measured sensitivities for the sensors as a function of input voltage. (d) Drift factor in sensor resistance for CNT and C-CNT sensors

Importantly, the drift significantly reduced at elevated temperature, as shown in figure 15(d). Equation (3) exhibits the drift factor, in which R_n is the heater resistance at the beginning of each sensing cycle and ΔR is the amount of increase in heater resistance when hydrogen gas is present. By using the drift factor equation (3), we can calculate how much

device resistance has been drifting as the sensing cycle goes on. The drift factor decreases for both as-deposited CNT and C-CNT sensors as input voltages increase, which means that the self-heating mechanism can lower the sensor drift due to the improvement of hydrogen gas desorption.

$$\text{Drift Factor} = (R_{(n+1)}\text{-}R_n) / \Delta R \times 100\ [\%] \quad (3)$$

Figure 16(a-b) shows the response of as-deposited CNT and C-CNT sensors in different concentrations of hydrogen gases at input voltage of 20 V. The sensitivities of both sensors linearly increase with hydrogen concentration. The rate of change for C-CNT sensors is about is about 2.6 times higher along with better linear dependency, meaning that the proposed C-CNT sensor is capable of detecting gas concentration as well as the presence of hydrogen gas. For varying hydrogen concentrations, both response time and recovery time of the sensors almost remained stable. In addition, we have analyzed the limit of detection (LOD) of the proposed CNT sensors using the root-mean-square deviation (RMSD) of the baseline signal, R_{rms} [5]. For calculating RMSD, we have used 100 data points and acquired using below the equation (4) that considers the signal to noise ratio larger than 3 as meaningful signals.

$$\text{LOD} = 3 \times R_{rms} / \text{Slope}\ [\text{ppm}] \quad (4)$$

The LODs from the measurement for CNT and C-CNT are 7100 ppm and 2700 ppm respectively. Even though LOD values of the proposed sensors are higher than that of the functionalized CNT based hydrogen sensors, it is still comparable to a previously reported LOD value [41]. Above all, C-CNT sensors shows 260 % enhancement in LOD as compared to as-deposited CNT sensors.

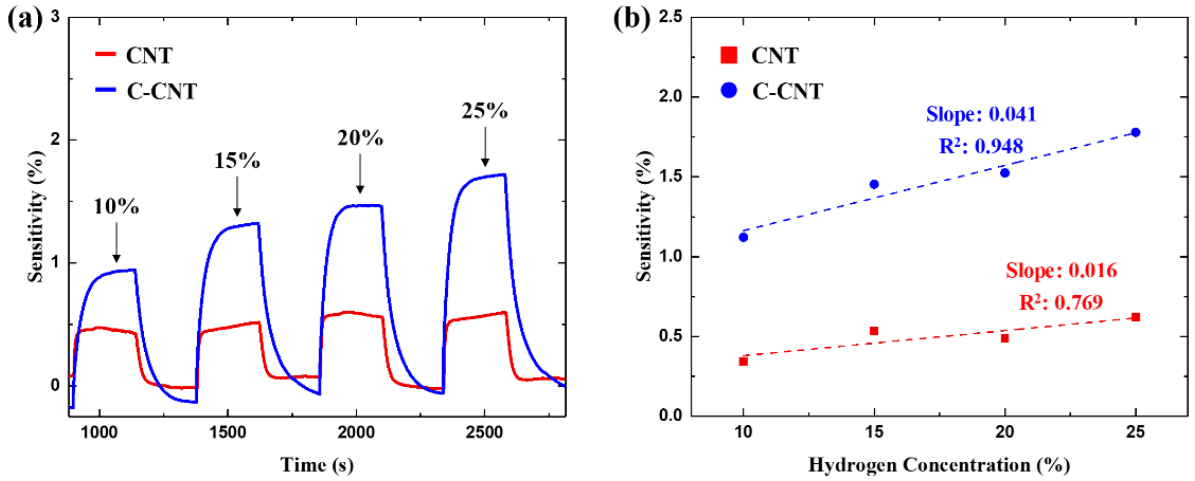

Figure 16. (a-b) Sensitivity of CNT and C-CNT sensors (V_{in} = 20V) at varying hydrogen concentrations. C-CNT sensors show a higher rate of change in measurement sensitivity compared to CNT sensors

To verify the repeatability of the C-CNT sensors, we have performed the hydrogen gas experiment for extended cycles. Figure 17(a) exhibits the response of as-deposited CNT and C-CNT sensors for 20 cycles of hydrogen sensing at 10 % concentration, which corresponds to about 3 hours. The overall shift in sensitivity is consistent under the whole measurement with small drift via self-heating of the sensors. Such well-developed performance shows that the C-CNT sensors can work for long periods with repeatable gas sensing measurements. Furthermore, we have fabricated at least four sensors with same fabrication process, and they have performed equivalent heating and sensing performances. This means that the fabrication of the suggested sensors is highly reproducible. It is also important to compare the heating characteristics of as-deposited CNT and C-CNT sensors before and after gas sensing. As shown in figure 17(b-c), both TCR and power to sensor temperature relations fairly remain stable, which confirms that our sensors possess high stability in terms of electro-thermal properties.

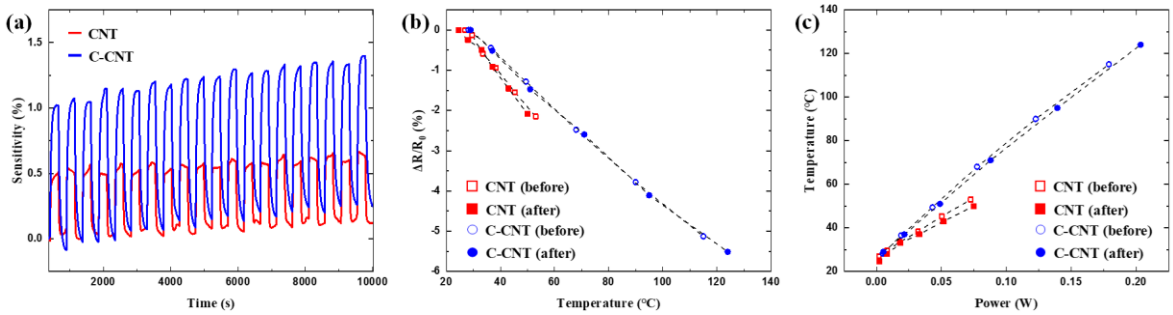

Figure 17. (a) Sensitivity of as-deposited CNT and C-CNT sensors with input voltage of 20 V for 20 cycles under hydrogen sensing at 10 % concentration. (b) Measured TCR and (c) power to sensor temperature before and after hydrogen sensing experiments.

5. Discussion

The presented C-CNT sensors utilize high CNT junction densities for efficient heating. Additionally, a self-heating mechanism of the sensors improves the measurement sensitivity and mitigates the sensor drift in hydrogen gas sensing. Table 1 compares the performances of the developed sensors to selected previous works on CNT based hydrogen gas sensors. From best of our knowledge, this work presents the utilization of crumpled CNT for the first time. Even though the measurement sensitivity and LOD of C-CNT sensors are rather limited compared to functionalized CNT sensors, we believe a proper functionalization process along with the design optimization could further enhance our device performance. In addition, many of previous works carry out external heating methods to improve the device sensitivity while our approach uses the sensor itself owing to the own heat source.

Table 2. Summary of CNT-based hydrogen gas sensors including the devices from this work

CNT type	Functionalization	Sensitivity	LOD	Heating	Reference
MWCNT	No	~0.4% (10% H_2)	7100 ppm	Self-heated (20 V, 42 ℃)	This work
Crumpled MWCNT	No	~1.3% (10% H_2)	2700 ppm	Self-heated (20 V, 73 ℃)	This work
MWCNT	No	~12% (18% H_2)	N/A	External (100 ℃)	[33]
MWCNT	Pd Pd/Pt	~4% (1% H_2) ~2% (1% H_2)	2000 ppm 400 ppm	No	[41]
MWCNT	MnO_2	~15% (18% H_2)	N/A	External (220 ℃)	[42]
MWCNT	Pt/TiO_2	~5% (20% H_2)	N/A	External (50 ℃)	[43]
MWCNT	Pt/f-GNPs	~17% (4% H_2)	N/A	No	[44]

When comparing the as-deposited CNT and C-CNT sensors, the measurement sensitivity is similar at a given heated temperature for as-deposited CNT and C-CNT sensors. However, C-CNT sensors exhibit more stable drift performance along with improved heating efficiencies, which is preferable for low-power or low-voltage applications. In addition, C-CNT sensors still demonstrate reliable operation along with higher measurement sensitivities, even without the self-heating of sensors. Such better sensing performances without heating highlight that the proposed C-CNT structures could be used to develop high performances room temperature gas sensors for single chemical detection applications [30].

Like other existing CNT based chemiresistive sensors, we need to consider several aspects for an accurate and reliable sensor operation. Since heater resistance depends on sensor temperature as well as the amount of hydrogen, it is essential to compensate and properly demonstrate the temperature effect from environments. For instance, 1 ℃ change in environmental temperature can induce 0.059 % shift in heater resistance, which could be

significant issue for pristine CNT based chemical sensors. In addition, humidity and other types of gases, such as CO, NO_2, CH_4, and O_2, also can affect the electrical resistance of CNTs [45]. Temperature or humidity issue could be addressed by integrating calibration sensors while the gas selectivity problems can be mitigated via functionalization with chemical agents [46-51]. Moreover, the proposed C-CNT sensor improves the rates of adsorption and desorption as compared to as-deposited CNT sensors without any chemical treatment. Hence, we believe the sensor performance would further improve via proper functionalization process to detect not only hydrogen, but also other chemicals.

6. Future work

To improve the sensitivity, response time, and recovery time, it is essential to scale down the device size [52]. Since the proposed thermal shrinkage can reduce the CNT area by about 400 % from the original size, even μm length scale C-CNT sensors can be realized by using a shadow mask with sub-mm feature sizes. As mentioned previously, the presented fabrication approach is scalable and allows a batch fabrication of C-CNT sensor arrays on a wafer scale.

Furthermore, higher self-heating temperatures would lead to enhanced sensitivities and drift performances based on our findings. A fabrication or transfer printing of C-CNT sensors onto thermally resistant substrate (Glass, Si, etc.) could lead to higher self-heated temperature, which would result in improved sensor performances. Finally, chemical or mechanical functionalization on C-CNT based sensors and improvement of sensor design could enhance in relation to not only sensitivity but also selectivity of various chemical gases.

All aforementioned approaches could further improve the current state of proposed C-CNT sensors, which exhibits superior heating efficiency, as detection sensitivity and repeatability, and less drift under long term sensing of hydrogen gas compared to as-deposited CNT sensors.

7. Conclusion

This paper proposes crumpled CNT (C-CNT) sensors with efficient self-heating abilities for high sensitivity and low drift hydrogen gas sensing. The fabrication process implements a rather simple spray coating to deposit a conformal layer of CNTs. In addition, a thermal shrinkage of Polystyrene (PS) substrate enables a reliable reproduction of C-CNT structures with high junction densities in a given area. The C-CNT sensors are more voltage and power efficient compared to as-deposited CNT devices. In addition, a highly linear TCR allows an accurate temperature measurement and control. In ambient environments, C-CNT sensors exhibit higher response to hydrogen than as-deposited CNT sensors. Furthermore, elevated sensing temperature via self-heating of the sensors increase both hydrogen adsorption and desorption rates, which ultimately improved the sensor performances while maintaining outstanding sensing repeatability and stability. Since the proposed C-CNT structures are more responsive to hydrogen and possess high heating efficiencies compared to the conventional as-deposited CNT sensors, C-CNT platforms could be applied towards an ultra-low power and high sensitivity hydrogen gas detection. In addition, the sensor itself works as a thermistor, and thus environment temperature fluctuations ca be addressed when necessary.

For future work, sub-mm scaled shadow masks allow C-CNT devices to be scaled down to μm-scale. Hence, we envision that the batch fabrication of C-CNT device arrays will be carried out on various wafer sizes ranging 2 to 6 inches. In addition, C-CNT structures will be transferred onto thermally resistant substrates, such as Silicon wafer, Glass or PET, so that we will be able to hydrogen gas detection as a function of higher temperature. Furthermore, when we transfer C-CNT structure to PET, we will be able to compare the power efficiency of C-CNT devices with that of as-deposited CNT

on same substrate. Utilizing SEM micrographs and Raman analysis, the analysis of C-CNT transfer printing could be done to study any chemical or mechanical effect from etching process. Lastly, with a proper chemical or mechanical functionalization and improved device design, we envision the application of C-CNT sensors to other chemical sensing applications beyond hydrogen gas detection.

8. References

[1] M. F. De Volder, S. H. Tawfick, R. H. Baughman, and A. J. Hart, "Carbon nanotubes: present and future commercial applications," *science*, vol. 339, no. 6119, pp. 535-539, 2013.

[2] S. Das, "A review on Carbon nano-tubes-A new era of nanotechnology," *Int J Emer Tech Adv Eng*, vol. 3, no. 3, pp. 774-783, 2013.

[3] D. Janas and K. Koziol, "A review of production methods of carbon nanotube and graphene thin films for electrothermal applications," *Nanoscale*, vol. 6, no. 6, pp. 3037-3045, 2014.

[4] V. Choudhary and A. Gupta, "Polymer/carbon nanotube nanocomposites," in *Carbon nanotubes-polymer nanocomposites*: IntechOpen, 2011.

[5] J. Li, Y. Lu, Q. Ye, M. Cinke, J. Han, and M. Meyyappan, "Carbon nanotube sensors for gas and organic vapor detection," *Nano letters*, vol. 3, no. 7, pp. 929-933, 2003.

[6] S.-I. Moon *et al.*, "Bias-heating recovery of MWCNT gas sensor," *Materials Letters*, vol. 62, no. 16, pp. 2422-2425, 2008.

[7] H.-S. Jang, S. K. Jeon, and S. H. Nahm, "The manufacture of a transparent film heater by spinning multi-walled carbon nanotubes," *Carbon*, vol. 49, no. 1, pp. 111-116, 2011.

[8] J.-W. Do *et al.*, "Solution-mediated selective nanosoldering of carbon nanotube junctions for improved device performance," *ACS nano*, vol. 9, no. 5, pp. 4806-4813, 2015.

[9] D. Jung, M. Han, and G. S. Lee, "Flexible transparent conductive heater using multiwalled carbon nanotube sheet," *Journal of Vacuum Science & Technology B, Nanotechnology and Microelectronics: Materials, Processing, Measurement, and Phenomena*, vol. 32, no. 4, p. 04E105, 2014.

[10] Y. Kim, H. R. Lee, T. Saito, and Y. Nishi, "Ultra-thin and high-response transparent and flexible heater based on carbon nanotube film," *Applied Physics Letters*, vol. 110, no. 15, p. 153301, 2017.

[11] S. Ji, W. He, K. Wang, Y. Ran, and C. Ye, "Thermal response of transparent silver nanowire/PEDOT: PSS film heaters," *Small*, vol. 10, no. 23, pp. 4951-4960, 2014.

[12] R. Menzel *et al.*, "Joule Heating Characteristics of Emulsion- Templated Graphene Aerogels," *Advanced Functional Materials*, vol. 25, no. 1, pp. 28-35, 2015.

[13] C. Celle, C. Mayousse, E. Moreau, H. Basti, A. Carella, and J.-P. Simonato, "Highly flexible transparent film heaters based on random networks of silver nanowires," *Nano Research*, vol. 5, no. 6, pp. 427-433, 2012.

[14] J. Bang *et al.*, "Assembly and densification of nanowire arrays via shrinkage," *Nano letters*, vol. 14, no. 6, pp. 3304-3308, 2014.

[15] S. J. Park, J. Kim, M. Chu, and M. Khine, "Highly flexible wrinkled carbon nanotube thin film strain

sensor to monitor human movement," *Advanced Materials Technologies*, vol. 1, no. 5, p. 1600053, 2016.

[16] S. J. Park, J. Kim, M. Chu, and M. Khine, "Flexible piezoresistive pressure sensor using wrinkled carbon nanotube thin films for human physiological signals," *Advanced Materials Technologies*, vol. 3, no. 1, p. 1700158, 2018.

[17] C. Cao *et al.*, "Highly Stretchable Supercapacitors via Crumpled Vertically Aligned Carbon Nanotube Forests," *Advanced Energy Materials*, vol. 9, no. 22, p. 1900618, 2019.

[18] Y. Wang and J. T. Yeow, "A review of carbon nanotubes-based gas sensors," *Journal of sensors*, vol. 2009, 2009.

[19] I. V. Zaporotskova, N. P. Boroznina, Y. N. Parkhomenko, and L. V. Kozhitov, "Carbon nanotubes: Sensor properties. A review," *Modern Electronic Materials*, vol. 2, no. 4, pp. 95-105, 2016.

[20] R. Tang, Y. Shi, Z. Hou, and L. Wei, "Carbon nanotube-based chemiresistive sensors," *Sensors*, vol. 17, no. 4, p. 882, 2017.

[21] M. Penza, P. J. Martin, and J. T. W. Yeow, "Carbon Nanotube Gas Sensors," in *Gas Sensing Fundamentals*, C.-D. Kohl and T. Wagner Eds. Berlin, Heidelberg: Springer Berlin Heidelberg, 2014, pp. 109-174.

[22] C. Wongchoosuk, A. Wisitsoraat, D. Phokharatkul, A. Tuantranont, and T. Kerdcharoen, "Multi-walled carbon nanotube-doped tungsten oxide thin films for hydrogen gas sensing," *Sensors*, vol. 10, no. 8, pp. 7705-7715, 2010.

[23] S. Young and Z. Lin, "Ethanol gas sensors based on multi-wall carbon nanotubes on oxidized Si substrate," *Microsystem Technologies*, vol. 24, no. 1, pp. 55-58, 2018.

[24] K. Chen *et al.*, "Printed carbon nanotube electronics and sensor systems," *Advanced Materials*, vol. 28, no. 22, pp. 4397-4414, 2016.

[25] A. D. Franklin *et al.*, "Sub-10 nm carbon nanotube transistor," *Nano letters*, vol. 12, no. 2, pp. 758-762, 2012.

[26] L. Xiang, H. Zhang, Y. Hu, and L.-M. Peng, "Carbon nanotube-based flexible electronics," *Journal of Materials Chemistry C*, vol. 6, no. 29, pp. 7714-7727, 2018.

[27] A. Abdelhalim, A. Abdellah, G. Scarpa, and P. Lugli, "Fabrication of carbon nanotube thin films on flexible substrates by spray deposition and transfer printing," *Carbon*, vol. 61, pp. 72-79, 2013.

[28] S. Kim, J. Yim, X. Wang, D. D. Bradley, S. Lee, and J. C. deMello, "Spin- and spray- deposited single- walled carbon- nanotube electrodes for organic solar cells," *Advanced Functional Materials*, vol. 20, no. 14, pp. 2310-2316, 2010.

[29] F. Wang, H. Gu, and T. M. Swager, "Carbon nanotube/polythiophene chemiresistive sensors for chemical warfare agents," *Journal of the American Chemical Society*, vol. 130, no. 16, pp. 5392-5393, 2008.

[30] L. Nguyen, P. Phan, H. Duong, C. Nguyen, and L. Nguyen, "Enhancement of NH3 gas sensitivity at room temperature by carbon nanotube-based sensor coated with Co nanoparticles," *Sensors*, vol. 13, no. 2, pp. 1754-1762, 2013.

[31] C. Wang, L. Yin, L. Zhang, D. Xiang, and R. Gao, "Metal oxide gas sensors: sensitivity and influencing factors," *Sensors*, vol. 10, no. 3, pp. 2088-2106, 2010.

[32] W.-D. Zhang and W.-H. Zhang, "Carbon nanotubes as active components for gas sensors," *Journal of Sensors*, vol. 2009, 2009.

[33] D. Jung, M. Han, and G. S. Lee, "Gas sensor using a multi-walled carbon nanotube sheet to detect hydrogen molecules," *Sensors and Actuators A: Physical*, vol. 211, pp. 51-54, 2014.

[34] W.-S. Cho, S.-I. Moon, Y.-D. Lee, Y.-H. Lee, J.-H. Park, and B. K. Ju, "Multiwall carbon nanotube gas sensor fabricated using thermomechanical structure," *IEEE Electron Device Letters*, vol. 26, no. 7, pp. 498-500, 2005.

[35] S. Gbordzoe, R. Malik, N. Alvarez, R. Wolf, and V. Shanov, "Flexible low-voltage carbon nanotube heaters and their applications," *Advances in Carbon Nanostructures*, pp. 123-136, 2016.

[36] D. Jung, D. Kim, K. H. Lee, L. J. Overzet, and G. S. Lee, "Transparent film heaters using multi-walled carbon nanotube sheets," *Sensors and Actuators A: Physical*, vol. 199, pp. 176-180, 2013.

[37] V. S. Turkani, D. Maddipatla, B. B. Narakathu, B. J. Bazuin, and M. Z. Atashbar, "A carbon nanotube based NTC thermistor using additive print manufacturing processes," *Sensors and Actuators A: Physical*, vol. 279, pp. 1-9, 2018.

[38] Y. Sun and H. H. Wang, "High- performance, flexible hydrogen sensors that use carbon nanotubes decorated with palladium nanoparticles," *Advanced Materials*, vol. 19, no. 19, pp. 2818-2823, 2007.

[39] M. S. Dresselhaus, G. Dresselhaus, R. Saito, and A. Jorio, "Raman spectroscopy of carbon nanotubes," *Physics reports*, vol. 409, no. 2, pp. 47-99, 2005.

[40] A. Maiti, "Carbon nanotubes: Bandgap engineering with strain," *Nature Materials*, vol. 2, no. 7, p. 440, 2003.

[41] L. Randeniya, P. Martin, and A. Bendavid, "Detection of hydrogen using multi-walled carbon-nanotube yarns coated with nanocrystalline Pd and Pd/Pt layered structures," *Carbon*, vol. 50, no. 5, pp. 1786-1792, 2012.

[42] D. Jung, Y. Yoon, and G. S. Lee, "Hydrogen sensing characteristics of carbon-nanotube sheet decorated

with manganese oxides," *Chemical Physics Letters,* vol. 577, pp. 96-101, 2013.

[43] L. De Luca *et al.*, "Hydrogen sensing characteristics of Pt/TiO2/MWCNTs composites," *international journal of hydrogen energy,* vol. 37, no. 2, pp. 1842-1851, 2012.

[44] A. Kaniyoor and S. Ramaprabhu, "Hybrid carbon nanostructured ensembles as chemiresistive hydrogen gas sensors," *Carbon,* vol. 49, no. 1, pp. 227-236, 2011.

[45] S. Arunachalam, A. Gupta, R. Izquierdo, and F. Nabki, "Suspended carbon nanotubes for humidity sensing," *Sensors,* vol. 18, no. 5, p. 1655, 2018.

[46] M. K. Kumar and S. Ramaprabhu, "Palladium dispersed multiwalled carbon nanotube based hydrogen sensor for fuel cell applications," *International Journal of Hydrogen Energy,* vol. 32, no. 13, pp. 2518-2526, 2007.

[47] I. Sayago *et al.*, "Carbon nanotube networks as gas sensors for NO2 detection," *Talanta,* vol. 77, no. 2, pp. 758-764, 2008.

[48] W. S. Lee and J. Choi, "Hybrid Integration of Carbon Nanotubes and Transition Metal Dichalcogenides on Cellulose Paper for Highly Sensitive and Extremely Deformable Chemical Sensors," *ACS applied materials & interfaces,* 2019.

[49] S.-J. Young and Z.-D. Lin, "Ethanol gas sensors composed of carbon nanotubes with Au nanoparticles adsorbed onto a flexible PI substrate," *ECS Journal of Solid State Science and Technology,* vol. 6, no. 10, pp. M130-M132, 2017.

[50] S. Young and Z. Lin, "Ammonia gas sensors with Au-decorated carbon nanotubes," *Microsystem Technologies,* vol. 24, no. 10, pp. 4207-4210, 2018.

[51] Z.-D. Lin, C.-H. Hsiao, S.-J. Young, C.-S. Huang, S.-J. Chang, and S.-B. Wang, "Carbon nanotubes with adsorbed Au for sensing gas," *IEEE Sensors Journal,* vol. 13, no. 6, pp. 2423-2427, 2013.

[52] M. Xiao *et al.*, "Batch fabrication of ultrasensitive carbon nanotube hydrogen sensors with sub-ppm detection limit," *ACS sensors,* vol. 3, no. 4, pp. 749-756, 2018.

요 약 문

수소 가스 센싱을 위한 고 효율성의 구겨진 탄소나노튜브 박막 히터

이 논문은 구겨진 탄소 나노 튜브 (C-CNT) 박막 히터 (Thin Film Heater)의 제조 및 고감도의 낮은 드리프트 (Drift) 수소 가스 센싱에 대한 응용을 제시한다. 다중 벽 탄소 나노 튜브 (MWCNT)의 용액을 간단한 스프레이 코팅 및 열 기판 수축 (Substrate Shrinkage) 방법을 이용하여, 밀접하게 접합 된 C-CNT 히터를 제조했습니다. C-CNT 의 줄 발열(Joule heating)은 기판 수축하지 않은 CNT 히터 (As-coated CNT)에 비해 같은 전압에서 더 높은 온도를 발생 시킵니다. 구체적으로는, C-CNT 히터의 온도는 주어진 영역에서 더 높은 접합 밀도로 인해 As-coated CNT 히터보다 200%만큼 증가합니다. 또한, C-CNT 및 As-coated CNT 히터의 온도 저항 계수 (Temperature Coefficient of Resistance, TCR)는 CNT 히터의 정확한 온도 제어 및 측정을 위해 분석됩니다. 다음과 같이 제작 된 모든 히터들은 높은 선형성의 TCR 을 보입니다.

C-CNT 히터의 고효율 가열 성능은 높은 흡착 및 탈착 특성을 가지고 있고, 이를 이용하여 수소 가스 센싱 (Hydrogen Gas Sensing)에 기여할 수 있습니다. C-CNT 히터는 수소 가스 감지가 가능하지만 As-coated CNT 히터에 비해 전기적 저항의 Drift 현상이 적고 측정 감도가 더 높습니다. 또한 제안 된 히터의 자체 가열 메커니즘은 수소의 빠른 탈착을 도와 반복적이고 안정적인 센서 작동을 가능하게 합니다. 이러한 연구 결과에서 C-CNT 형태와 가열 온도가 모두 수소 감지 성능에 영향을 미치는 것으로 밝혀졌습니다. 제안 된 C-CNT 장치는 저전력 또는 저전압 감지 플랫폼에서 활용 될 수 있습니다.

향후 작업에서는 1 mm 이하 사이즈의 쉐도우 마스크를 사용하게 되면, C-CNT 디바이스를 μm 스케일로 축소 할 수 있습니다. 따라서, 2 내지 6 인치 범위의 다양한 웨이퍼 크기에서 정렬된 C-CNT 디바이스를 일괄적으로 공정이 가능할 수 있을 것으로 예상합니다. C-CNT 구조층을 실리콘 웨이퍼, 유리, 또는 PET 와 같은 내열성 기판으로 전사 작업을 하게 되면 200 ℃ 이상의 고온에 따른 수소 가스 검출을 확인 할 수 있습니다. 또한, C-CNT 구조 층을 PET 에 전사 작업을 하게 되면 동일한 기판 상에 증착된 CNT 와 직접적으로 비교할 수 있을 것으로 기대합니다. 전자작업중에 발생 할 화학적 또는 물리적인 영향을 검사하기 위해 주사전자현미경 사진과 라만 분광 분석을 활용하여 분석을 수행 할 수 있습니다. 마지막으로, 적절한 화학적 또는 물리적인 금속 기능화 (Metal Functionalization)와 개선된 디바이스 디자인을 통해 수소 가스 검출 이외의 다른 화학 감지 적용 분야에 C-CNT 센서를 적용 할 수 있을 것으로 기대합니다.

핵심어: 다중 벽 탄소나노튜브 (MWCNTs), 박막 히터 (Thin Film Heater), 줄 발열 (Joule Heating), 기판 수축 (Substrate Shrinkage), 수소 가스 센싱 (Hydrogen Gas Sensing)

Appendix

1 Polymer Substrate and MWCNTs Specification

1.1 PET Film

- Manufacturer: Graphene Square
- Area: 200 mm × 200 mm
- Thickness: 188 μm

1.2 Polystyrene Film

- Manufacturer: GRAFIX
- Area: 210 mm × 297 mm
- Thickness: 254 μm

1.3 MWCNTs

- Manufacturer: US Research Nanomaterials, Inc
- Outer and Inner Diameter: 5 -15 nm / 3 -5 nm
- Concentration: 3 wt%
- Length: 50 μm
- Solvent: Water

2 Ultrasonicator and Air-spray Gun Specification

2.1 Ultrasonicator

- Manufacturer & Model: HWASHIN / 510
- Applied Frequency & Power: 40 kHz / 400 Watt
- Operated Time: 1 Hour
- Temperature of Ultrasonicator: Room Temperature

2.2 Air-spray Gun and Compressor

- Air-spray Gun Manufacturer & Model: SPARMAX / GP-35
- Compressor Manufacturer & Model: SPARMAX / TC-501
- Applied Air Pressure: 2.4 bar
- Flow Rate: 0.4 mL/sec
- Spraying Height: 15 cm
- Temperature of Hotplate: 70 ℃

3 Raman Spectra

3.1 Raman Spectroscopy

- Manufacturer & Model: NanoBase / XperRam 200
- Laser Wavelength: 532 nm
- Applied Power: 0.1 mWatt
- Exposure Time: 20 sec

4 Metal Deposition (Sputtering)

4.1 Dielectric Sputtering System

- Manufacturer / Model: SORONA / SRN-110
- Power (Gold & Platinum) : 300 Watt
- Argon Pressure (Gold & Platinum): 6 mTorr / 9 mTorr
- Deposition Time (Gold & Platinum): 210 sec / 275 sec

5 Experimental Setup for Hydrogen Sensing

5.1 Vacuum-probe Station

- Manufacturer & Model: MSTECH / M5VC
- Pressure in Chamber: 400 mTorr
- Total Gas Flow Rate (Ar:H_2): 500 sccm (450 sccm : 50 sccm)
- Temperature in Chamber: Room Temperature

5.2 LABVIEW Block Diagram

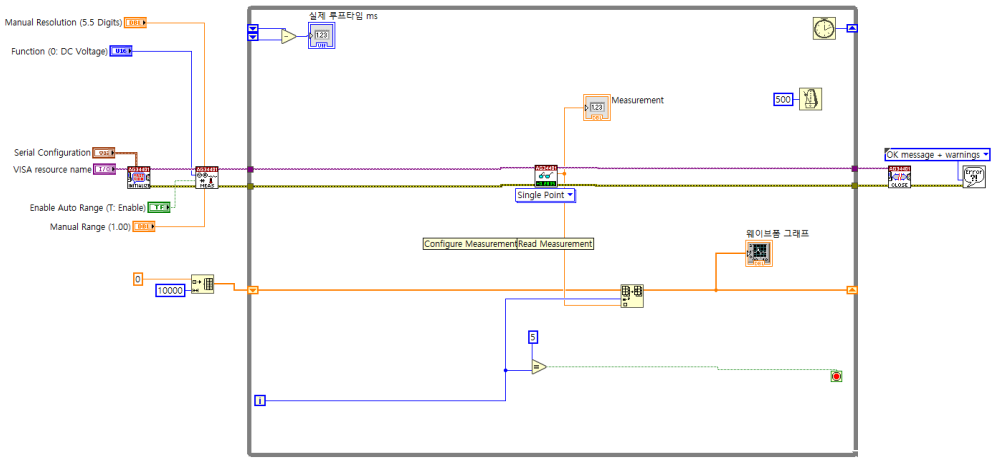

5.3 Sensor Loading

- Spacing: 0.5 cm

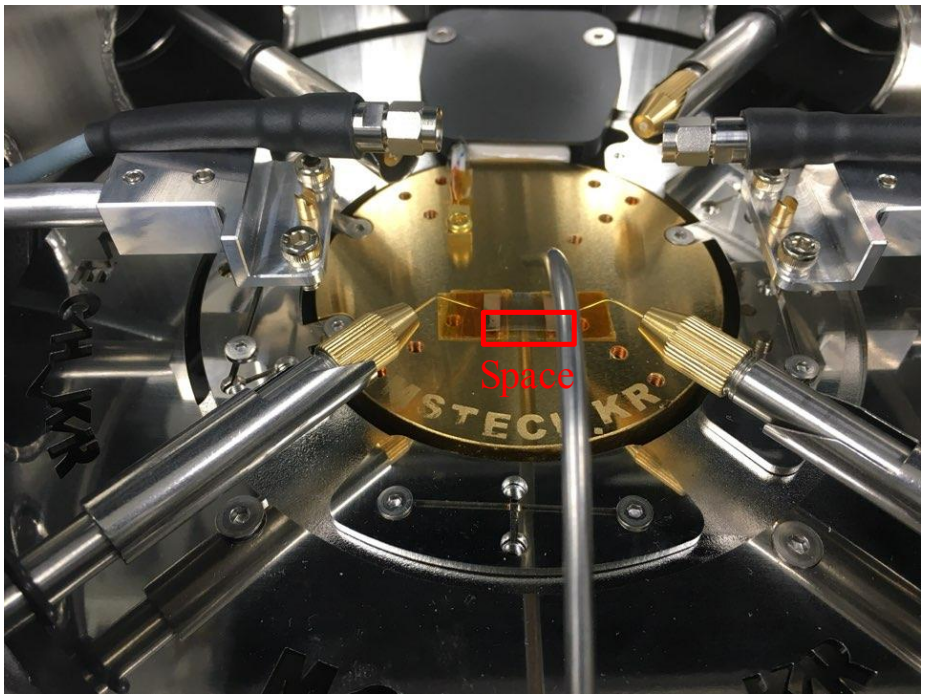

5.4 Photograph for Gas Sensing and LABVIEW Operation